ionic conductivity in microporous structures.

Acknowledgment. We wish to thank Dr. M. Tsai for valuable discussion in ionic conductivities and Prof. W. McCarroll for his helpful comments. This is publication No. D10550-6-91 of the New Jersey Agricultural Experiment Station supported by State Funds and the Center for Advanced Food Technology (CAFT). The Center for Advanced Food Technology is a New Jersey Commission on Science and Technology Center.

Registry No. $(NH_4)_3HGe_7O_{16}\cdot 6H_2O$, 139311-81-2; $Li_3HGe_7O_{16}\cdot 6H_2O$, 139311-80-1; $K_3HGe_7O_{16}\cdot 4H_2O$, 12395-61-8; $Rb_3HGe_7O_{16}\cdot 4H_2O$, 12529-64-5; $Cs_3HGe_7O_{16}\cdot 4H_2O$, 139311-82-3; $K_3HGe_7O_{16}$, 12195-29-8; $Rb_3HGe_7O_{16}$, 12195-32-3; $Cs_3HGe_7O_{16}$, 12191-09-2; $Li_6Ge_8O_{19}$, 51912-96-0; $Li_3HGe_7O_{16}$, 12195-30-1.

Preparation, Characterization, and Ionic Conductivity of Novel Crystalline, Microporous Silicogermanates, $M_3HGe_{7-m}Si_mO_{16}\cdot xH_2O$, M = K^+, Rb^+, Cs^+; $0 < m < 3$; $x = 0$–4. 3

Shouhua Feng, Menting Tsai, Sung-Ping Szu, and Martha Greenblatt*

Department of Chemistry, Rutgers, The State University of New Jersey, Piscataway, New Jersey 08855-0939

Received November 20, 1991. Revised Manuscript Received January 14, 1992

Crystalline, microporous silicogermanates, $M_3HGe_{7-m}Si_mO_{16}\cdot xH_2O$, M = K^+, Rb^+, and Cs^+, $0 < m < 3$, $x = 0$–4, were synthesized from hydrothermal systems and characterized by powder X-ray diffraction, differential thermal and thermogravimetric analysis, Fourier transform infrared, and solid-state ^{29}Si nuclear magnetic resonance techniques. Ionic conductivity in dehydrated samples was investigated by ac impedance in the temperature range 25–550 °C. The framework substitution of Si for Ge at tetrahedral positions leads to a significant increase of ionic conductivity and decrease of activation energy. The effects of the silicon content and size of ionic radius on the activation energy and ionic conductivity are discussed.

1. Introduction

In previously reported work[1,2] on the preparation and ionic conductivity of a series of crystalline, microporous germanates, $M_3HGe_7O_{16}\cdot xH_2O$, M = Li^+, NH_4^+, Na^+, K^+, Rb^+, and Cs^+, we found that the dehydrated samples have better ionic conductivity than the traditional zeolites. The cubic framework structure of the germanates is built up of face- and edge-sharing GeO_6 octahedra which corner share with GeO_4 tetrahedra (Figure 1). There are three four-coordinated and four six-coordinated Ge atoms in the unit cell. Four out of sixteen framework oxygen atoms are four-coordinated by Ge atoms and a hydrogen atom, which is located in the center of the cell.[3] There are channels of eight-membered rings with a window size of ~4.3 Å in the [100] direction that contain the mobile cations and water molecules. It was shown that these materials with mixed GeO_4–GeO_6 polyhedra forming a framework structure have potential applications as molecular sieves, ion-conducting electrolytes, and humidity sensing materials. However, compared with typical fast ion conductors,[4,5] the activation energy for ionic conduction in these materials is higher, which lowers the ionic conductivity in the low temperature range. In this present work, we attempt to improve the conductivity in the germanates via substitution of SiO_4 for GeO_4. The substitution of Si^{4+} for Ge^{4+} is expected to weaken the electrostatic interaction between mobile cations and the framework oxygens because the Si–O bond is more covalent, which polarizes the oxygen charge density more strongly toward the Si atoms so as to give the framework oxide ions a lower effective negative charge.

Here we report the results of the hydrothermal crystallization, structural characterization, and ionic conductivity of $M_3HGe_{7-m}Si_mO_{16}\cdot xH_2O$, M = K^+, Rb^+, and Cs^+, $0 < m < 3$.

2. Experimental Section

$M_3HGe_{7-m}Si_mO_{16}\cdot xH_2O$, M = K^+, Rb^+, and Cs^+ were directly synthesized hydrothermally at 180–200 °C in sealed systems containing an aqueous mixture of MOH, the α-quartz form of germanium dioxide, and SiO_2 sol. A typical synthesis began with the combination of GeO_2 (Eagle-Picher Co., reagent grade) and the aqueous solution of alkali metal hydroxide (KOH, RbOH, or CsOH, Fisher, reagent grade) to form an aqueous solution; SiO_2 sol (AESAR, Johnson Matthey INC) was added to the first solution. Crystallization of the aqueous gel was carried out in stainless steel autoclaves lined with poly(tetrafluoroethylene) (PTFE) under autogenous pressure at empirically determined temperatures. The crystalline product was filtered, washed with distilled water and dried at ambient temperature.

The powder X-ray diffraction (XRD) patterns were recorded on a Scintag X-ray diffractometer with monochromatized Cu Kα radiation. Unit-cell parameters were obtained with a least-squares method, with silicon as an internal standard. The analysis of Si content was carried out on a Beckman Spectrometric Spectraspan IIIB DCT Basic Multi dc argon plasma emission spectrometer. Differential thermal analysis (DTA) and thermogravimetric analysis (TGA) were carried out on a Du Pont Model 9900 thermal analyzer with a heating rate of 10 °C/min in air. Fourier transform infrared (FTIR) spectra were recorded at room temperature on

* To whom correspondence should be addressed.

(1) Feng, S.; Tsai, M.; Greenblatt, M. *Chem. Mater.*, in press.
(2) Feng, S.; Greenblatt, M. *Chem. Mater.*, previous paper in this issue.
(3) Nowotny, H.; Wittmann, A. *Monatsh. Chem.* **1954**, *85*, 561.
(4) Goodenough, J. B.; Hong, H. Y.-P.; Kafalas, J. A. *Mater. Res. Bul.* **1976**, *11*, 203.
(5) Hong, H. Y.-P. *Mater. Res. Bul.* **1978**, *13*, 117.

0897-4756/92/2804-0468$03.00/0

Table I. Hydrothermal Synthetic Conditions for $M_3HGe_{7-m}Si_mO_{16}\cdot 4H_2O$, M = K^+, Rb^+, and Cs^+

run no.	M_2O/GeO_2	SiO_2/GeO_2	H_2O/M_2O	crystallization temp, °C	crystallization time, days	crystalline product
KSI01	1.0	0.40	120	200	7	$K_3HGe_{5.4}Si_{1.6}O_{16}\cdot 4H_2O$
KSI02	1.0	0.50	120	200	7	$K_3HGe_{4.8}Si_{2.2}O_{16}\cdot 4H_2O$
KSI03	1.0	0.67	120	200	7	$K_3HGe_{4.5}Si_{2.5}O_{16}\cdot 4H_2O$
RBS03	0.8	0.67	120	200	10	$Rb_3HGe_{4.8}Si_{2.2}O_{16}\cdot 4H_2O$
CSS03	0.8	0.67	120	200	10	$Cs_3HGe_{4.9}Si_{2.1}O_{16}\cdot 4H_2O$

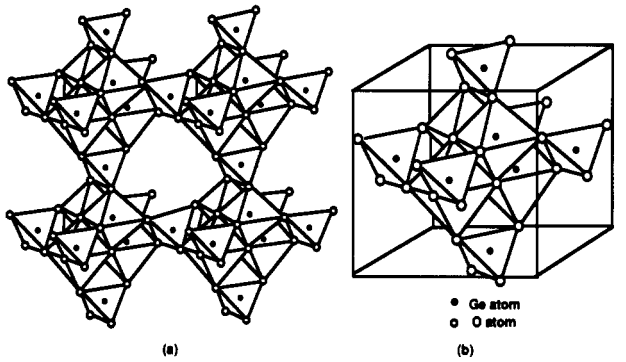

Figure 1. (a) Framework structure of $M_3HGe_7O_{16}\cdot 4H_2O$ and (b) the unit cell, illustrating the GeO_4 tetrahedra and GeO_6 octahedra linkages.

a Perkin-Elmer infrared Fourier transform spectrometer (Model 1720) on samples in KBr pellets at room temperature in the range 400–4000 cm^{-1} with 2-cm^{-1} resolution. ^{29}Si nuclear magnetic resonance (NMR) spectra were recorded on a Varian VXR-200 spectrometer equipped with a Doty magic angle spinning (MAS) probe in a 47-kG field at 39.75 MHz. A simple one-pulse sequence was used for obtaining the ^{29}Si spectra. The recycle time between pulses was 180 s. Chemical shift was relative to tetramethylsilane (TMS).

Ionic conductivities were measured by ac impedance technique using a Solartron Model 1250 frequency analyzer and 1186 electrochemical interface that are equipped with a Hewlett-Packard 9816 desktop computer for data collection and analysis. Disk-shaped samples were prepared by a pelletizing pressure of 100 klb/in.^{2}. Electrode connection to the samples was made by coating the faces of the pellets with platinum ink. A frequency range of 10 Hz to 65 kHz and a heating rate of 2 °C/min were used throughout. The dehydrated samples were preheated at different temperatures (depending on sample) and then cooled in Ar prior to the ac impedance measurements, which were also carried out in flowing dry Ar gas.

3. Results and Discussion

3.1. Synthesis. The initial composition and synthetic conditions for K, Rb, and Cs silicogermanates are listed in Table I. $M_3HGe_{7-m}Si_mO_{16}\cdot xH_2O$ can be crystallized from the starting mixtures with molar composition range of $(0.5–1.5)M_2O\cdot(0.4–0.7)SiO_2\cdot GeO_2\cdot(50–150)H_2O$ at 200 °C. The structure unit (Figure 1) of the parent germanate is composed of three GeO_4 tetrahedra and four GeO_6 octahedra per unit cell. In basic conditions Si tends to have a four-coordinated environment and therefore the substitution of Ge in tetrahedral position by Si would be expected. The Si content in the initial composition is critical for the synthesis of pure phases; the alkaline content determines the crystallinity of the product. The synthesis of a completely substituted silicon analogue has not been successful; a SiO_2/GeO_2 ratio larger than 1 in the starting composition led to the formation of impurity SiO_2 phase. Analysis of Si content in the products shows that the maximum number of Si atom in the formula (m) is less than 3.

3.2. Structural Characterization. 3.2.1. XRD. Figure 2 shows the X-ray diffraction patterns for K, Rb, and Cs silicogermanates. All samples are pure phases, and

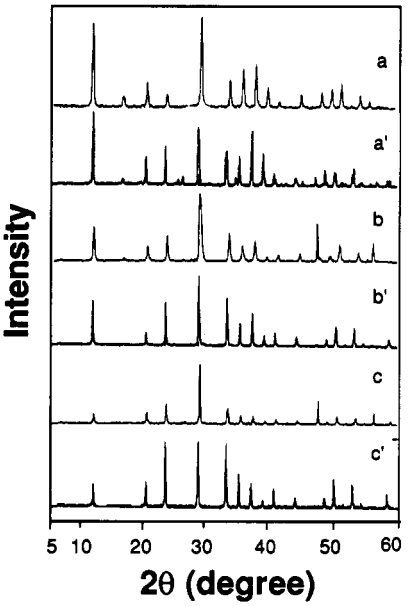

Figure 2. Powder X-ray diffraction patterns for (a) $K_3HGe_{4.8}Si_{2.2}O_{16}\cdot 4H_2O$, (a') $K_3HGe_7O_{16}\cdot 4H_2O$, (b) $Rb_3HGe_{4.8}Si_{2.2}O_{16}\cdot 4H_2O$, (b') $Rb_3HGe_7O_{16}\cdot 4H_2O$, (c) $Cs_3HGe_{4.9}Si_{2.1}O_{16}\cdot 4H_2O$, and (c') $Cs_3HGe_7O_{16}\cdot 4H_2O$.

Table II. Unit Cell Parameters for Germanates and Silicogermanates (Space Group: $P\bar{4}3m$)

sample	a, Å	V, Å^3
$K_3HGe_7O_{16}\cdot 4H_2O$	7.720 (0)	460.1
$K_3HGe_{5.4}Si_{1.6}\cdot 4H_2O$	7.566 (9)	433.1
$K_3HGe_{4.8}Si_{2.2}O_{16}\cdot 4H_2O$	7.524 (2)	425.9
$K_3HGe_{4.5}Si_{2.5}O_{16}\cdot 4H_2O$	7.512 (2)	423.1
$Rb_3HGe_7O_{16}\cdot 4H_2O$	7.722 (5)	460.5
$Rb_3HGe_{4.8}Si_{2.2}O_{16}\cdot 4H_2O$	7.621 (2)	442.6
$Cs_3HGe_7O_{16}\cdot 4H_2O$	7.734 (3)	462.6
$Cs_3HGe_{4.9}Si_{2.1}O_{16}\cdot 4H_2O$	7.726 (1)	461.2

the X-ray patterns are similar to those for the corresponding parent germanates, but the peaks in each pattern shift to higher degree (2θ). The cell parameters are listed in Table II. The a unit cell parameters for the silicogermanates are smaller than those for the parent compounds, and as the silicon content increases, the a unit cell parameter decreases as in the case of K silicogermanates.

3.2.2. DTA-TGA. DTA analyses shows that the decomposition temperatures of $M_3HGe_{7-m}Si_mO_{16}\cdot xH_2O$, M = K^+ (m = 2.2), Rb^+ (m = 2.2), and Cs^+ (m = 2.1), are 720, 750, and 700 °C, respectively, which are ~40–50 °C higher than those of the Si-free compounds.[2] The endothermic peaks in the temperature range 50–200 °C are due to dehydration. Figure 3 shows the TG heating–cooling curves indicating various weight losses on heating and absorption of water on cooling. The TG cooling curves for the $M_3HGe_{7-m}Si_mO_{16}\cdot xH_2O$, M = K^+, Rb^+, and Cs^+, indicate that dehydrated samples absorb water reversibly at different absorption rates. The total weight loss of water for $M_3HGe_{7-m}Si_mO_{16}\cdot xH_2O$, M = K^+ (m = 2.2), Rb^+ (m = 2.2), and Cs^+ (m = 2.1), are 9.3, 8.7, and 5.7%, respectively, corresponding to $x \sim 4 \pm 0.9$.

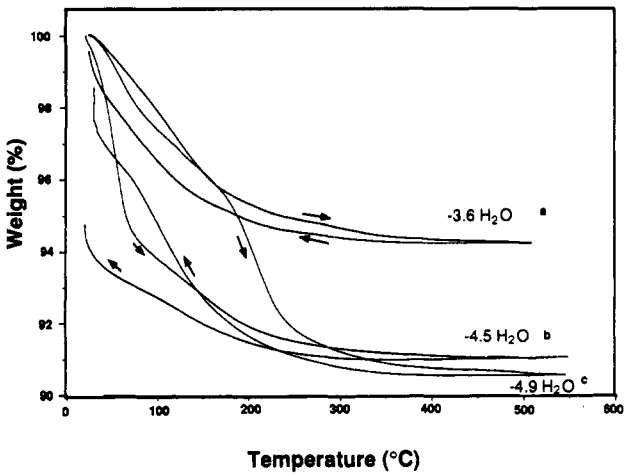

Figure 3. TG analyses for (a) $Cs_3HGe_{4.9}Si_{2.1}O_{16}\cdot 4H_2O$, (b) $Rb_3HGe_{4.8}Si_{2.2}O_{16}\cdot 4H_2O$, and (c) $K_3HGe_{4.8}Si_{2.2}O_{16}\cdot 4H_2O$ showing both heating and cooling curves.

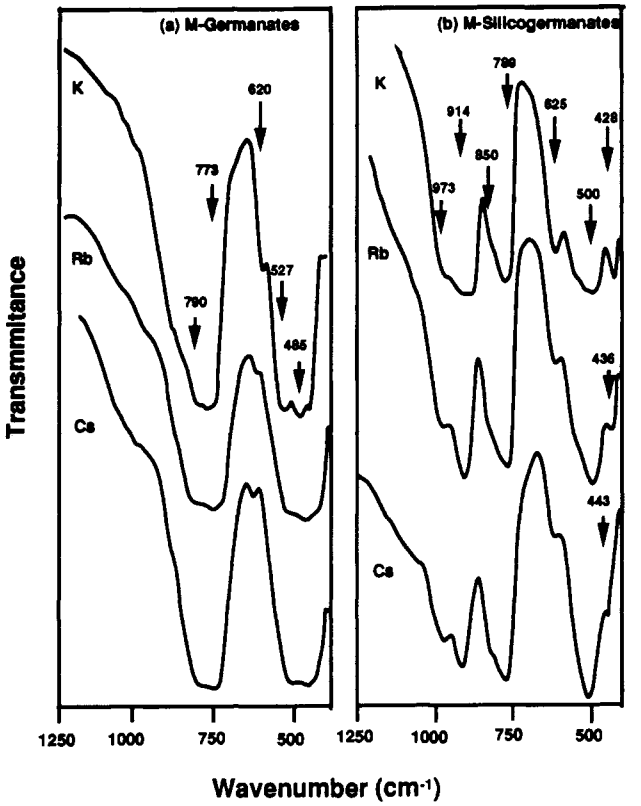

Figure 4. FTIR spectra for (a) M germanates and (b) M silicogermanates, M = K, Rb, and Cs.

3.2.3. FTIR. The FTIR spectra of the germanates and the Si substituted analogues shown in Figure 4, respectively, are substantially different. In the IR spectra of the germanates, the strong bands at 773 and 790 cm^{-1} have been assigned to the asymmetric stretching vibrations of internal Ge–O and external Ge–O–Ge linkages, respectively.[6] The bands at 527 and 620 cm^{-1} have been attributed to the symmetric stretching motion of Ge–O and Ge–O–Ge, respectively.[7] A Ge–O bending vibration was also observed at 485 cm^{-1}. The vibrations of GeO_6 octahedra ovelap with some of the GeO_4 tetrahedral vibrations. In the FTIR spectra for silicogermanates, there are additional absorptions at 914 and 973 cm^{-1} which can be assigned to the asymmetric stretching vibrations of Si–O and Si–O–Ge, respectively, similar to those observed in aluminosilicate zeolites.[8] The Ge–O and Ge–O–Ge asymmetric stretching bands at 789 and 850 cm^{-1}, respectively, are observed in the silicogermanates, but the intensity of these bands is reduced compared to the unsubstituted phases and corresponds to the decrease of Ge content due to Si substitution. All of the bands observed in the FTIR spectra of silicogermanates shift to higher frequency, compared with those for their parent germanates, which indicate that there are stronger bonds in the silicogermanate framework structure, which is consistent with the increase of thermal stability of silicogermanates as indicated by the DTA. In the FTIR spectra of silicogermanates, the sharp bands at 428–443 cm^{-1} (which are not clear in the FTIR spectra of the germanates) are related to pore vibrations sensitive to the cations in the channels, as observed in the IR spectra of zeolites.[8] The blue shift of the absorption in this region from K^+ to Cs^+ shows that the electrostatic interaction between framework oxygen and cations decreases as cation radius increases. This observation is in agreement with the weakening of electrostatic interaction between framework oxygen and mobile cations by substitution of Si for Ge.

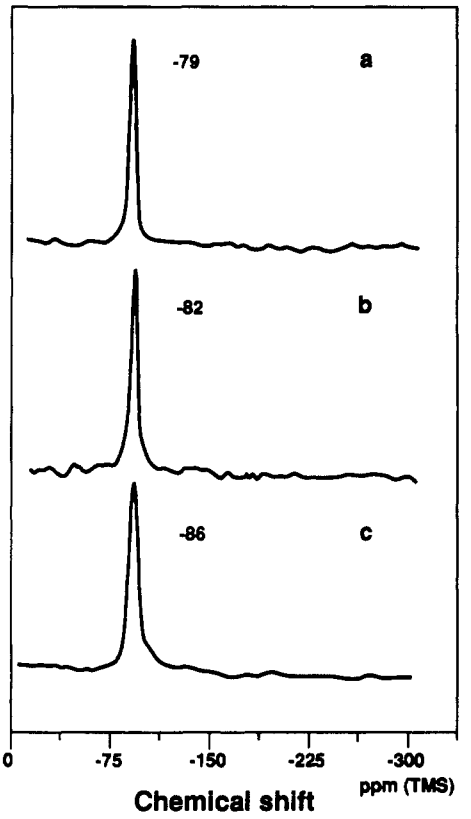

Figure 5. ^{29}Si MAS NMR spectra for (a) $K_3HGe_{4.8}Si_{2.2}O_{16}\cdot 4H_2O$, (b) $Rb_3HGe_{4.8}Si_{2.2}O_{16}\cdot 4H_2O$, and (c) $Cs_3HGe_{4.9}Si_{2.1}O_{16}\cdot 4H_2O$. TMS is used as reference.

3.2.4. ^{29}Si MAS NMR. Figure 5 shows the ^{29}Si solid-state NMR spectra of K, Rb, and Cs silicogermanates with chemical shifts −79, −82, and −86 ppm, respectively. The NMR assignment of ^{29}Si Q(0), Q(1), Q(2), Q(3), and Q(4) species (i.e. silicon tetrahedra with zero, one, two, three,

(6) Paques-Ledent, M. Th. *Spectrochim. Acta* **1976**, *32A*, 383.
(7) Tarte, P.; Pottier, M. J.; Proces, A. M. *Spectrochim. Acta* **1973**, *29A*, 1017.
(8) Flanigen, E. M. Structural Analysis by Infrared Spectroscopy. In *Zeolite Chemistry and Catalysis*; Rabo, L. A., Ed.; ACS Monograph 171; American Chemical Society: Washington, DC, 1976; p 80.
(9) Lippma, E.; Magi, M.; Samoson, A.; Tarmak, M.; Engehardt, G. *J. Am. Chem. Soc.* **1981**, *103*, 4992.

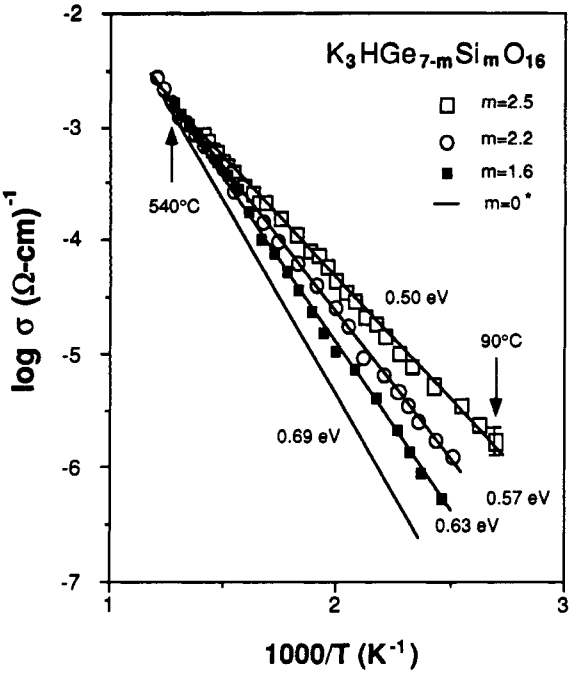

Figure 6. Temperature dependence of conductivity of $K_3HGe_{7-m}Si_mO_{16}$, m = 2.5, 2.2, 1.6, and 0. * The data with m = 0 are from ref 2.

and four nearest-neighbor aluminum, Si(0Al), Si(1Al), Si(2Al), Si(3Al), and Si(4Al)) for aluminosilicate zeolites is well-known.[10] The NMR signals in Figure 5 correspond to tetrahedral Si corner sharing four GeO_6 octahedra [Q(4)] (see Figure 1). The change in chemical shift observed for K, Rb, and Cs silicogermanates can be attributed to differences in electrostatic interactions of different cations with the framework oxygens near the six-coordinated Ge atoms. Smith et al. have found a correlation between the isotropic chemical shift and the total framework cation-oxygen bond strength.[10] Because the K^+ is more polarizing than Rb^+ or Cs^+, the total framework cation–oxygen bond strength is weaker in the K^+ compound than in the Rb^+ or Cs^+ analogues. This results in a more positive chemical shift in the K^+ compound.

3.3. Ionic Conductivity of Dehydrated Samples. Figure 6 shows the temperature dependence of conductivity for dehydrated K silicogermanate with different silicon contents. Figure 7 shows the temperature dependence of conductivity for dehydrated Rb and Cs silicogermanates with similar Si contents. Prior to the conductivity measurement the pellet sample was dehydrated by preheating it to 550 °C and then cooling in dry Ar. The relationship between log conductivity (σ) and the reciprocal of the absolute temperature is linear over the temperature range measured. The activation energies (E_a) were obtained from the Arrhenius plots, using the relationship

$$\sigma T = \sigma_0 e^{-E_a/kT} \quad (1)$$

where σ_0 is the preexponential factor, k Boltzmann's constant, and T absolute temperature. In general, E_a is composed of two energy terms: one to generate defect sites in the crystal (E_f) and another one necessary for the ions to overcome potential barriers during migration (E_m). For microporous materials the number of thermally generated defect sites is small in comparison with the number of existing structural empty sites; therefore, the activation energy obtained mainly represents the value of the potential barriers, E_m. It is noted from Figure 6 that the conductivity of each K silicogermanate is higher than that of the Si-free K germanate below 540 °C, where the lines intersect. The conductivity results are consistent with the weakening of the electrostatic interactions between framework oxygens and mobile cations. Because the Si–O bonds are more covalent, the oxygen charge density is polarized more strongly toward the Si atoms so as to give the framework oxide ions a lower effective negative charge, and thereby in the Si-substituted phase weakening the electrostatic interaction between mobile cations and the framework oxygens. This is supported by FTIR analysis. The weaker framework–mobile cation interaction facilitates faster cation motion. The activation energy of conductivity for $K_3HGe_{7-m}Si_mO_{16}$ decreases with increasing

(10) Smith, K. A.; Kirkpatrick, R. J.; Oldfield, E.; Henderson, D. M. *Am. Mineral.* **1983**, *68*, 1206.

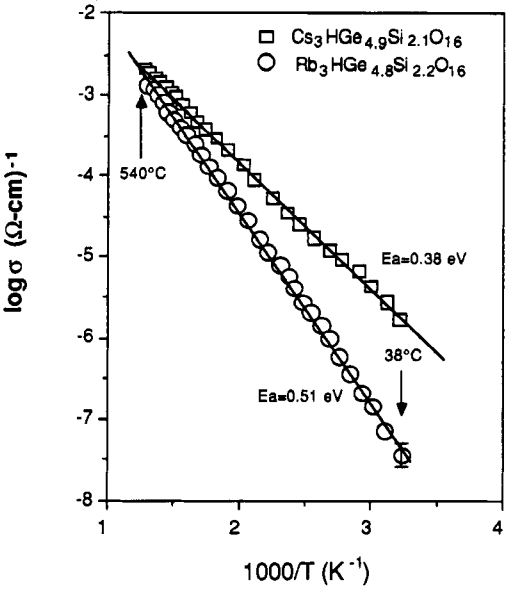

Figure 7. Temperature dependence of conductivity of $Cs_3HGe_{4.9}Si_{2.1}O_{16}$ and $Rb_3HGe_{4.8}Si_{2.2}O_{16}$.

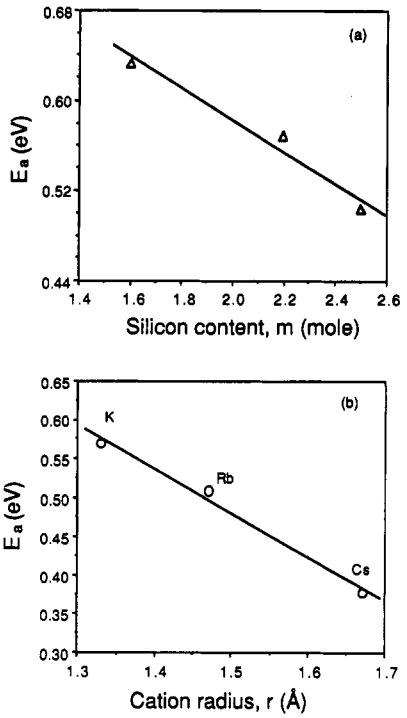

Figure 8. (a) Activation energy versus silicon content for $K_3HGe_{7-m}Si_mO_{16}$. (b) Activation energy versus cation radius for $M_3HGe_{7-m}Si_mO_{16}$, M = K^+, Rb^+, and Cs^+.

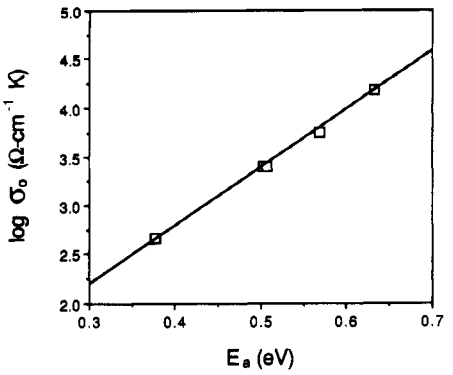

Figure 9. Logarithm of preexponential factor versus activation energy of $M_3HGe_{7-m}Si_mO_{16}$, $M = K^+$ (m = 1.6, 2.2, and 2.5), Rb^+ (m = 2.2), and Cs^+ (m = 2.1).

silicon content (Figure 8a). This further confirms the role of Si as weakening the electrostatic interactions between the framework oxygens and cations in the channels. With increasing Si content, the decreasing activation energy dominates the ion mobility and the conductivity increases, even though the concentration of cations has not changed (Figure 6). The correlation of activation energy with increasing radius of cation in the channels, as shown in Figure 8b, is not unexpected, because the Coulombic attraction between the cations and the negatively charged framework decreases with increasing cation radius (K^+, 1.33 Å; Rb^+, 1.47 Å; Cs^+, 1.67 Å).

The variation of the logarithm of the preexponential factor (σ_0) versus the activation energy is linear as shown in Figure 9, which can be fitted with the equation proposed by Almond and West:[11,12]

$$\log \sigma_0 = S/k + \log (K\omega_0) \quad (2)$$

$$S = E_a/T^* \quad (3)$$

where S is the entropy for conduction, K a carrier concentration term, ω_0 the fundamental vibration frequency of the mobile ions, and T^* the effective disordering temperature in the mobile ion sublattice. Above T^*, the order–disorder transition temperature, the mobile cations are disordered over their lattice sites and other sites that link up to form the conduction paths. The slope ($1/kT^*$) of the line in Figure 9 corresponds to a value of T^* = 580 °C. This value of T^* is in fairly good agreement with T^* = 540 °C obtained from the intercept of Arrhenius plots for a series of $M_3HGe_{7-m}Si_mO_{16}$ phases (Figures 6 and 7). These results support Almond and West's hypothesis that the large variations often observed in the preexponential factors (σ_0) of solid electrolytes with similar structure and constant mobile cation content (as the case here) is dominated by the entropy of activation. Thus it appears that the predominant factor governing ionic conduction above T^* is the entropy of activation.

(11) Almond, D. P.; West, A. R. *Solid State Ionics* **1987**, *23*, 27.
(12) Almond, D. P.; Duncan, G. K.; West, A. R. *Solid State Ionics* **1983**, *8*, 159.

4. Conclusions

In summary, crystalline, microporous silicogermanates, $M_3HGe_{7-m}Si_mO_{16}\cdot xH_2O$, $M = K^+$, Rb^+, and Cs^+ and $0 < m < 3$ were synthesized from hydrothermal systems. The characterization by XRD, DTA-TGA, FTIR and ^{29}Si solid-state NMR techniques shows that the silicon atoms are in tetrahedral positions in the framework structure. The substitution of Si for Ge in the structure leads to a decrease of activation energy and to an increase of ion conductivity. These effects are attributed to the weakening of electrostatic interactions between the negatively charged framework and mobile cations. The activation energy scales with both the Si content and the cation size.

Acknowledgment. We thank Dr. R. Fuller for his critical reading of this paper. This is publication No. D10550-7-91 of the New Jersey Agricultural Experiment Station supported by State Funds and the Center for Advanced Food Technology (CAFT). The Center for Advanced Food Technology is a New Jersey Commission on Science and Technology Center.

Registry No. $K_3HGe_7O_{16}\cdot 4H_2O$, 12395-61-8; $K_3HGe_{5.4}Si_{1.6}O_{16}\cdot 4H_2O$, 139242-37-8; $K_3HGe_{4.8}Si_{2.2}O_{16}\cdot 4H_2O$, 139242-39-0; $K_3HGe_{4.5}Si_{2.5}O_{16}\cdot 4H_2O$, 139242-33-4; $Rb_3HGe_7O_{16}\cdot 4H_2O$, 12529-64-5; $Rb_3HGe_{4.8}Si_{2.2}O_{16}\cdot 4H_2O$, 139242-41-4; $Cs_3HGe_7O_{16}\cdot 4H_2O$, 139311-82-3; $Cs_3HGe_{4.9}Si_{2.1}O_{16}\cdot 4H_2O$, 139242-36-7; $K_3HGe_{4.5}Si_{2.5}O_{16}$, 139242-32-3; $K_3HGe_{4.8}Si_{2.2}O_{16}$, 139242-38-9; $K_3HGe_{5.4}Si_{1.6}O_{16}$, 139242-34-5; $Cs_3HGe_{4.9}Si_{2.1}O_{16}$, 139242-35-6; $Rb_3HGe_{4.8}Si_{2.2}O_{16}$, 139242-40-3.